

# An intrinsically fluorescent glycoligand for direct imaging of ligand trafficking in artificial and living cell systems

Cite this: DOI: 10.1039/c3nj00380a

Ludivine Garcia,<sup>a</sup> Mirca Lazzaretti,<sup>b</sup> Antoine Diguët,<sup>cde</sup> Francesca Mussi,<sup>b</sup> Franco Bisceglie,<sup>f</sup> Juan Xie,<sup>g</sup> Giorgio Pelosi,<sup>f</sup> Annamaria Buschini,<sup>b</sup> Damien Baigl<sup>cde</sup> and Clotilde Policar<sup>\*cdh</sup>

Received (in Montpellier, France)  
10th April 2013,  
Accepted 8th July 2013

DOI: 10.1039/c3nj00380a

[www.rsc.org/njc](http://www.rsc.org/njc)

Glycoligands, sugar-based molecules able to complex metal cations, constitute a new class of molecules with great potential for biological and biochemical applications. To analyze their behaviour in a biological environment, we have synthesized an intrinsically fluorescent glycoligand and analyzed its trafficking in both living (U937 human cancer cells) and artificial (giant unilamellar vesicles) cell systems. We have found that this ligand has moderate cytotoxicity accompanied by specific accumulation in both living and reconstituted membranes, which it can cross to reach inner compartments.

## 1. Introduction

Glycoligands are a new family of metal binding ligands constituted of appended Lewis bases on a sugar platform. Carbohydrates have been shown to be useful molecular tools to design ligands and complexes for asymmetric catalysis,<sup>1–4</sup> as metalloenzyme biomimetics<sup>5,6</sup> or siderophore mimetics,<sup>7</sup> to control metal properties such as magnetic anisotropy,<sup>8</sup> the chirality of Cu(II) in mononuclear<sup>9,10</sup> and dinuclear species,<sup>11</sup> and to generate selective chelators, which can be of interest for biological application.<sup>12,13</sup> Carbohydrates also are valuable central platforms to develop biologically active compounds: their ready availability, biocompatibility and easy poly-functionalisation providing access to chemical diversity are assets to develop bioactive compounds.

To improve the design and to understand the bio-activity of glycoligands, there is a need to characterize their distribution to different organs, tissues, or cell types, to study their cell-penetration properties, and interaction with biological membranes, to provide insights into the cellular uptake, and to follow their distribution

between organelles inside a given cell. Among different possible techniques, fluorescence is particularly well suited for cell-imaging. It is possible to append a fluorescent moiety to the molecule to be tracked. This approach has been successfully applied by conjugating a variety of fluorescent probes including synthetic organic fluorophores (*e.g.*, fluorescein,<sup>14</sup> NBD,<sup>15,16</sup> rhodamine<sup>15</sup>), inorganic nanoparticles (*e.g.*, quantum dots<sup>17</sup>) and fluorescent proteins.<sup>18</sup> However, such a conjugation may induce a modification of the physico-chemical properties, such as polarity, acidity, metal affinity or hydrophobicity. As a result, both distribution and functionality of the conjugated molecule inside the cell can be dramatically affected compared to the original un-conjugated molecule. An alternative is to use intrinsically fluorescent compounds, that is, the fluorescent probe being a part of the molecule of interest that can then be directly mapped inside cells, as in a few examples in the literature.<sup>19,20</sup> Benzothiadiazole is a particularly interesting candidate for fluorescence imaging as it fluoresces in the visible range.<sup>12,21,22</sup> Despite its attractive characteristics, it has been seldom used for bio-imaging.<sup>23–25</sup>

Therefore, to get further insight into the behaviour of glycoligands, we combined a cytotoxicity analysis with an imaging approach using an intrinsically fluorescent glycoligand containing a benzothiadiazole moiety,<sup>12</sup> and a dual imaging approach using both living cell membranes and reconstituted membranes. We used U937 human cancer cells as living cells and giant unilamellar vesicles (GUVs) as they are commonly used as robust and well-defined artificial cell model systems.<sup>26</sup>

Compound **1** (Scheme 1) is soluble in water and is made of a *ribo*-furanose scaffold with triazolylpyridyl and triazolyl-benzothiadiazolyl moieties. Its absorption and fluorescence

<sup>a</sup> Univ. Paris-Sud 11, ICMMO, Equipe de Chimie Bioorganique et Bioinorganique, F-91405 Orsay Cedex, France

<sup>b</sup> Università degli Studi di Parma, Dipartimento di Bioscienze, 43124 Parma, Italy

<sup>c</sup> Department of Chemistry, Ecole Normale Supérieure, 24, rue Lhomond, 75005 Paris, France. E-mail: [clotilde.policar@ens.fr](mailto:clotilde.policar@ens.fr); Fax: +33 1 44 32 33 97; Tel: +33 1 44 32 24 20

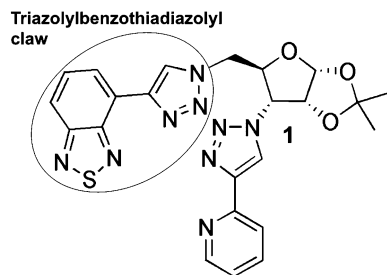
<sup>d</sup> Université Pierre et Marie Curie Paris 6, 4 Place Jussieu, 75005 Paris, France

<sup>e</sup> Laboratoire PASTEUR UMR 8640, CNRS, France

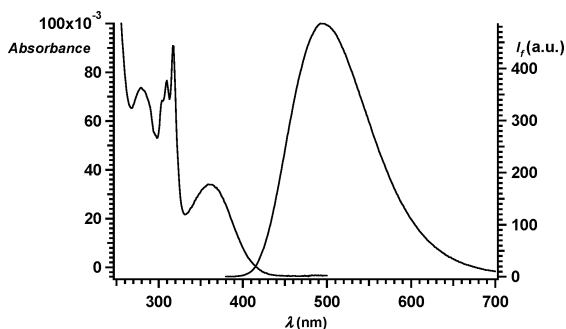
<sup>f</sup> Università degli Studi di Parma, Dipartimento di Chimica, 43124 Parma, Italy

<sup>g</sup> PPSM, Institut d'Alembert, ENS Cachan, CNRS, 61 av Président Wilson, F-94230, Cachan, France

<sup>h</sup> Laboratoire des BioMolécules, UMR7203, CNRS, France



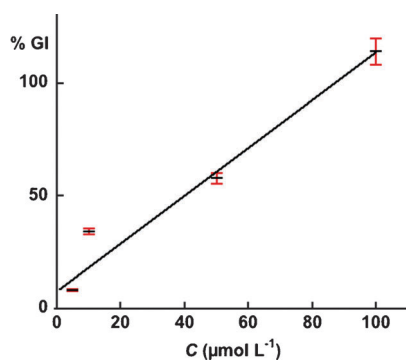
Scheme 1 Glycoligand 1.

Fig. 1 Absorption and fluorescence spectra of **1** at  $c = 8 \mu\text{mol L}^{-1}$  in a mixture of water–DMSO (85 : 15),  $\lambda_{\text{exc}} = 368 \text{ nm}$  (for spectra in other solvents, see ref. 12).

spectra in water–DMSO (85/15) are shown in Fig. 1. Upon excitation at 368 nm, it was found to exhibit a maximum of emission at 510 nm (water–DMSO) and an exceptionally high quantum yield of 94%.<sup>12</sup> Its physico-chemical properties are very similar to other derivatives conjugated with a benzothiadiazole moiety.<sup>12,21,27</sup>

## 2. Cellular cytotoxicity

First, compound **1** was assayed against the U937 cells for its antiproliferative effect. Cytotoxicity was analyzed by measuring cell proliferation by MTS assay. The dose–response curve clearly highlighted a dose-related inhibition of cell growth (Fig. 2). Compound **1** induced a decrease in the proliferative activity of

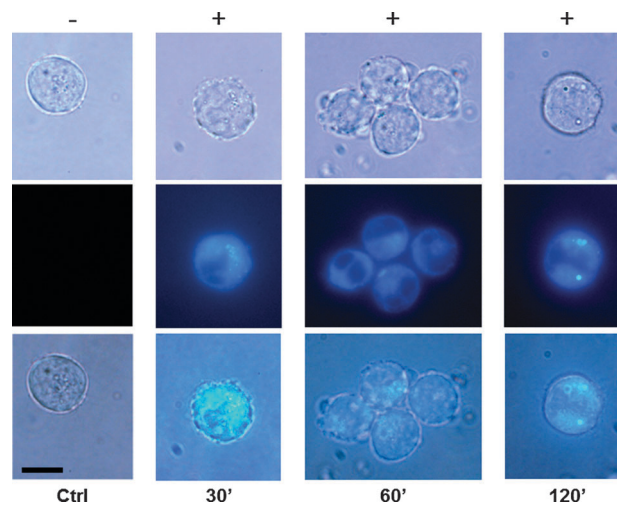
Fig. 2 Plot of cell growth inhibition (GI) in U937 after treatment with **1** (with error bars in red). The solid line represents the linear regression best fit. Symbols and error bars show mean  $\pm$  SD (quadruplicate, see Experimental part).

the U937 cell line; the  $\text{IC}_{50}$  (50% inhibitory concentration) after 24 h of incubation was  $40 \pm 2 \mu\text{M}$ .

To be cytotoxic a molecule needs to reach an appropriate cellular target and hence cytotoxicity is closely related to the cell-penetration property. The  $\log P$ -value is defined as the ratio of the concentrations of a compound in a biphasic mixture of water and octanol, with  $\log P = \log(C_{\text{octanol}}/C_{\text{water}})$ . Ideally, to penetrate cells, a compound should be amphiphilic with a  $\log P$ -value between 2 and 5. A value above 5 corresponds to a too lipophilic compound unable to cross and then get out of membranes, whereas a value below 2 indicates a too hydrophilic compound that would not get inside membranes.<sup>28</sup> The  $\log P$ -value for compound **1** was estimated using a computational method<sup>29,30</sup> to be  $2.5 \pm 0.8$ . This value indicates a lipophilicity that is adequate for cell penetration.<sup>28</sup>

## 3. Cell imaging

The cellular incorporation of **1** was then tested *in vitro* on the U937 cell line. Briefly, cells were incubated at the  $\text{IC}_{50}$  concentration ( $40 \mu\text{M}$ ) of **1** in culture medium (RPMI with *L*-glutamine 1%, FBS 10%, penicillin/streptomycin 1%) and the evolution of both cellular morphology and distribution of **1** was followed by microscopy over a 2 hour period. Fig. 3 shows representative phase contrast, fluorescence and merged images of cells as a function of incubation time. First, for each incubation time, a control experiment (Ctrl) performed in the absence of **1** showed a normal membrane morphology and the absence of any fluorescence signal. This shows that cells exhibited a normal physiology with no auto-fluorescence under the conditions used to image **1** in the absence of **1**. In contrast, in the presence of **1**, phase contrast observations evidenced some morphological changes while the distribution of **1** could be simultaneously detected by fluorescence. From these observations, some main pieces of information can be obtained. First, all cells exhibited a much higher fluorescence than the background, indicating a significant intracellular

Fig. 3 U937 cells after 30, 60 or 120 min incubation with medium (Ctrl) or **1** at  $40 \mu\text{M}$  (+); the same cells were detected in optical phase contrast (first line) and under fluorescence (second line). The third line shows the merged images. Scale bar  $10 \mu\text{m}$ .

accumulation of **1**. In most cells, the nucleus remained dark, which shows that **1** was mainly accumulating in the cytoplasm. The fluorescence intensity did not change much from 30 min to 120 min of incubation, showing that, once **1** had been incorporated, it was not released anymore by the cell, with a steady-state cellular concentration reached at *ca.* 30 min. Then, the cytoplasm exhibited a diffuse fluorescence with some brighter fluorescence spots indicating an accumulation at some particular locations. The density of these fluorescent spots increased with time. These spots may be a sign of a local accumulation of **1** probably in specific subcellular structures or a precipitation. Finally, the formation of some blebs at the plasma membrane was observed. It is noteworthy that these blebs were never fluorescent showing that **1** was not incorporated in these sub-structures as observable in the merged images (Fig. 3). All these results show that using an intrinsically fluorescent glycoligand such as **1** enabled us to simultaneously follow both its effect on the response of a live cell (*e.g.*, morphological changes) and its intracellular distribution over incubation time.

#### 4. Artificial cell imaging

To have an insight into the interaction of compound **1** with the cellular membrane, we studied the behaviour of **1** in the presence of giant unilamellar vesicles (GUVs). GUVs are constituted of a closed phospholipid bilayer with a diameter in the range 1–200  $\mu\text{m}$ . These vesicles are convenient to investigate the membrane properties as they are easy to prepare and to observe with conventional light microscopy techniques.<sup>31</sup> GUVs were made of egg phosphatidylcholine (EPC) phospholipids and prepared by electroformation in sucrose.<sup>32–34</sup> After sedimentation in an isotonic solution of **1** (20  $\mu\text{M}$ ) in glucose, GUVs were characterized by confocal microscopy. Fig. 4A shows representative images of GUVs after 140 min of incubation. Regardless of presence or absence of **1**, all GUVs displayed the usual spherical morphology and a diameter ranging from 5 to 150  $\mu\text{m}$ . This shows that **1** did not affect the size distribution and morphology of GUVs.

GUVs in the presence of **1** exhibited a strong fluorescence peak at their membrane contour. Fig. 4B shows characteristic fluorescence intensity profiles along different individual GUVs. In the absence of **1**, no signal can be detected from the background. In the presence of **1**, the background intensity was significantly increased, which is due to the fluorescence of **1**. Moreover, for all GUVs, a characteristic peak in fluorescence intensity was observed at the exact position of the membrane. The intensity of this peak was similar for all GUVs and was approximately twice that of the background. This shows a local accumulation of **1** in GUV membranes, which is in agreement with the lipophilicity of **1**. Interestingly, the intensity inside each GUV was comparable to the background outside the GUV and much higher than the background in the absence of **1**.

This result shows that **1** crossed the membrane during incubation to accumulate inside GUVs until an equilibrium was reached when the concentration of **1** inside the GUVs became similar to that outside. To further investigate the incorporation of **1**, we characterized more precisely the interior of the GUVs by confocal microscopy. It is known that, during electroformation, a small

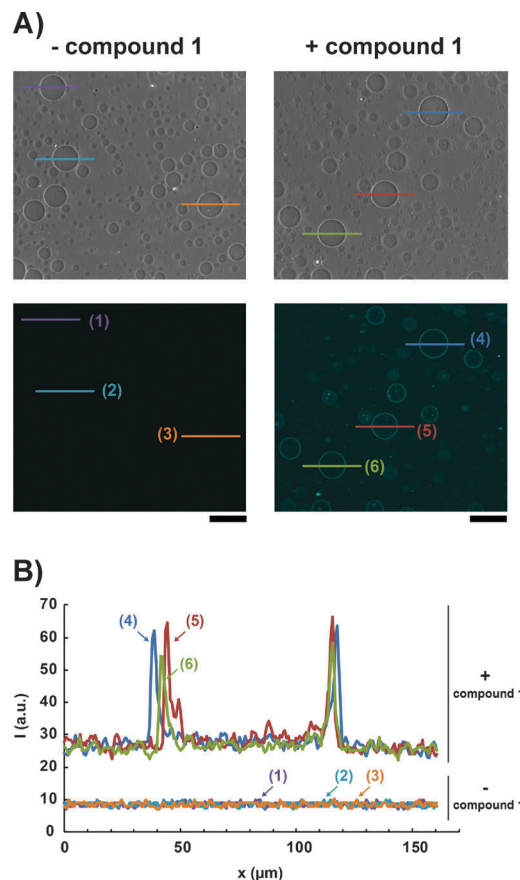


**Fig. 4** Confocal microscopy images of GUVs made of egg phosphatidylcholine (EPC) after sedimentation and incubation for 140 min in a glucose solution with (+) or without (–) compound **1** (20  $\mu\text{M}$ ). (A) Representative phase contrast (top) and fluorescence (bottom) images of GUVs. (B) Fluorescence intensity profile along lines shown in (A). Scale bar 100  $\mu\text{m}$ .

fraction of GUVs contains smaller vesicles. These inner vesicles were indeed observed before incubation with **1**, and we wanted to know whether **1**, after crossing the outer GUV membrane, was able to reach these inner vesicles. Fig. 5 shows typical close-ups of individual GUVs. Interestingly, when inner vesicles were present inside GUVs (see arrows in Fig. 5), they always displayed a fluorescence signal comparable to the outer membrane of the corresponding GUV. This observation indicates that **1** was not only accumulating in the external membrane but was also able to enter the inner aqueous-compartment to reach the inner vesicles. Although the formation of inner vesicles induced by **1** could not be excluded, we have never observed any invagination or endocytosis-like events upon addition of **1**. All these results demonstrate the ability of **1** to traffick in cell-like compartments with a specific accumulation depending on the local polarity of the medium. This can be related to its intermediate  $\log P$ -value close to 2, indicative of a lipophilic compound but with an ability to be soluble in water.

All the results on GUVs show how an intrinsically fluorescent glycoligand such as **1** accumulates in a cell membrane model which can be crossed enabling a distribution in both the inner and outer compartments.

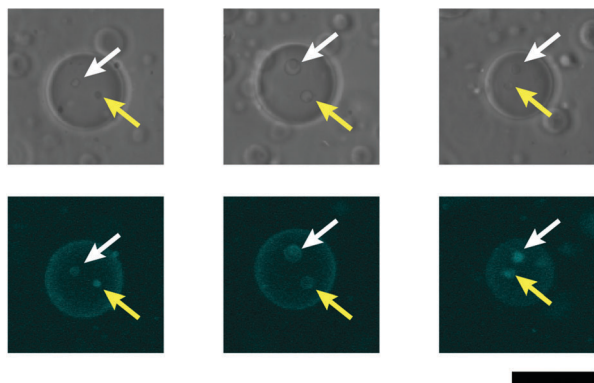


**Fig. 5** Confocal microscopy images of individual GUVs in phase contrast (top) and fluorescence (bottom) modes after sedimentation and incubation for 140 min in a glucose solution with compound **1** (20  $\mu\text{M}$ ). Arrows indicate small vesicular structures inside the main GUV. Scale bar 50  $\mu\text{m}$ .

## 5. Experimental part

### 5.1 Human cells

The histiocytic lymphoma (U937) cell lines were obtained from the American Tissue Culture Collection (Rockville, MD). Cell lines were maintained in the exponential phase at 37  $^{\circ}\text{C}$  in a 5% carbon dioxide atmosphere using RPMI-1640 medium (Lonza, Verviers, Belgium) with 25 mM HEPES buffer containing 10% fetal calf serum (Lonza, Verviers, Belgium), antibiotics (50 units  $\text{mL}^{-1}$  penicillin and 50  $\mu\text{g mL}^{-1}$  streptomycin), and 2 mM L-glutamine.

### 5.2 Cytotoxicity assays: MTS test

The growth inhibitory effects toward the U937 tumor cell line was evaluated by means of MTS (tetrazolium salt reduction) assay (CellTiter96<sup>R</sup> AQueous One Solution Cell Proliferation Assay – Promega Corporation, Madison, WI, USA). First of all, a calibration curve of absorbance against the cell number was constructed (Fig. 6). For treatment,  $5 \times 10^3$  cells per well were seeded in 96-well microplates in growth medium (100  $\mu\text{L}$ ) and then incubated at 37  $^{\circ}\text{C}$  in a 5% carbon dioxide atmosphere. After 24 h, the compound to be studied was added at the appropriate concentrations. Quadruplicate cultures were established for each treatment. After 24 h, the cytotoxicity assay

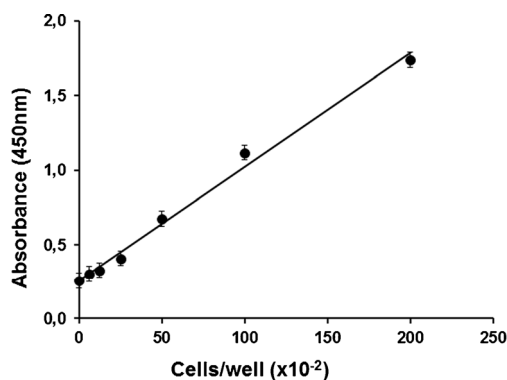


**Fig. 6** Effect of the cell number on absorbance at 450 nm measured using the MTS assay and best linear regression.

was performed by adding 20  $\mu\text{L}$  of the CellTiter96<sup>R</sup> AQueous One Solution Cell Proliferation Assay directly to culture wells, incubating for 4 h and then recording the absorbance at 450 nm with a 96-well plate reader (MULTISKAN EX, Thermo Electron Corporation, Vantaa, Finland).

Mean absorbance at 450 nm (formazan) for each compound-dose in quadruplicate was expressed as a percentage of the untreated control well absorbance and plotted vs. drug concentration. IC<sub>50</sub> values represent the drug concentrations that reduced the mean absorbance at 450 nm to 50% of those in the untreated control wells after a 24 h-incubation.

### 5.3 GUV preparation and observation

For all the experiments, the same electroformation procedure was applied. First, 4  $\mu\text{L}$  of a 10  $\text{mg mL}^{-1}$  solution of egg phosphatidylcholine (EPC) in chloroform was spread at a constant speed with a micropipette tip on an indium tin oxide (ITO) electrode substrate previously cleaned by isopropyl alcohol and acetone. After the phospholipid film was dried,  $\sim 400 \mu\text{L}$  of a swelling aqueous solution containing  $\sim 0.1 \text{ M}$  sucrose, 4.6 mM  $\text{NaN}_3$  was introduced between the two electrodes, separated by a silicon rubber spacer. Electroformation was performed using a sinusoidal AC field (2 V and 10 Hz) for 3 h.

The vesicle suspension was then extracted under low shear stress and mixed in a PDMS well with a similar volume of a solution containing  $\sim 0.1 \text{ M}$  glucose, 4.6 mM  $\text{NaN}_3$ , previously adjusted to have the same osmolarity as that of the sucrose solution (111 mOsm). The vesicles mixed with the glucose solution were then collected by gravity on a microscope glass slide after 2 h of decantation and observed using optical microscopy.

### 5.4 Microscopy

**Cells.** Briefly, U937 cells at a concentration of  $5 \times 10^4$  cells per mL were seeded in a 24-well plate (250  $\mu\text{L}$  per well). After 24 hours compound **1** was added for 30, 60 and 120 minutes. Then, 30  $\mu\text{L}$  of cell suspension were dripped onto a glass slide, smeared and fixed by incubating in 4% paraformaldehyde in PBS. Finally, one drop of mounting medium (VECTASHIELD<sup>®</sup> without DAPI) was used to fix the coverslip before microscopic evaluation. Fluorescence was observed using a DAPI filter set (exc. 330–380 nm, em. above 470 nm).

**GUVs.** To check the GUV production, phase-contrast microscopy was performed using an Axioobserver D1 inverted microscope (Zeiss), equipped with an EM-CCD camera (Photonmax 512B, Princeton Scientific). To compare the fluorescence of ligands in the inner and the outer media of the GUV, a confocal microscope was used (Fv10i, Olympus, using a laser excitation at 405 nm and emission in the range 420–460 nm). To investigate the interaction of **1** with the living U937 cells, a fluorescence microscope was used (Eclipse E600, Nikon). Morphological changes were assessed in bright field, while the distribution of the fluorescence was achieved by a DAPI filter set which is appropriate to observe compound **1**, as indicated by the spectra in absorption and emission, showing characteristics close to DAPI.

## 6. Conclusions

In conclusion, we observed that the intrinsically fluorescent glycoligand **1** showed a biological activity that resulted in a weak cytotoxicity. Its endogenous fluorescence enabled the study of its distribution and interaction with membranes in both living and artificial cell systems. The benzothiadiazole moiety was obviously an efficient low-molecular weight probe for fluorescence imaging in the visible range. It was thus possible to directly observe cell uptake of **1** and map its distribution in living cells allowing us to assess that **1** is cell-permeating and accumulates inside cells inducing chemical stress. The study of the interaction of **1** with the reconstituted model membranes provided by GUVs evidenced two main properties: (i) **1** locally accumulates at outer and inner membranes, showing that it can be used as a membrane probe and (ii) **1** is able to passively cross membranes to reach the inner compartments. The combination of the data from experiments in living cells and in GUVs provides a further insight into the cell-penetration properties of compound **1**. This study demonstrates that intrinsically fluorescent glycoligands such as **1** will constitute in future useful platforms to study *in situ* the bio-physico-chemical characteristics (e.g., complexation, catalytic activity) of the glycoligand moiety while being able to simultaneously get information on the ligand trafficking behaviour in artificial or living cell systems.

## Funding sources

CP wishes to acknowledge the French government for the starting grant "Jeune chercheur" JC4044. CP and LG wish to acknowledge the *Groupe d'intérêt scientifique Métalloprotéines et modèles* for supporting LG's mobility to Italy for the cell experiments.

## Notes and references

- 1 E. Raluy, M. Diéguez and O. Pamies, *J. Org. Chem.*, 2007, **72**, 2842–2850.
- 2 R. Del Litto, V. Benessere, F. Ruffo and C. Moberg, *Eur. J. Org. Chem.*, 2009, 1352–1356.
- 3 F. Ruffo, R. D. Litto, A. D. Roma, A. D'Errico and S. Magnolia, *Tetrahedron: Asymmetry*, 2006, **17**, 2265–2269.
- 4 A. Mako, D. K. Menhyhard, P. Bako, K. György and L. Toke, *J. Mol. Struct.*, 2008, **892**, 336–342.
- 5 T. Tanase, H. Inukai, T. Onaka, M. Kato, S. Yano and S. J. Lippard, *Inorg. Chem.*, 2001, **40**, 3943–3953.
- 6 R. Wegner, M. Gottschaldt and H. Görls, *Angew. Chem., Int. Ed.*, 2000, **39**, 595–599.
- 7 S. Dhungana, S. Heggemann, L. Heinisch, U. Möllmann, H. Boukhalfa and A. L. Crumbliss, *Inorg. Chem.*, 2001, **40**, 7079–7086.
- 8 G. Charron, F. Bellot, F. Cisnetti, G. Pelosi, J.-N. Rebilly, E. Rivière, A.-L. Barra, T. Mallah and C. Policar, *Chem.-Eur. J.*, 2007, **13**, 2774–2782.
- 9 F. Cisnetti, R. Guillot, M. Thérissod, M. Desmadril and C. Policar, *Inorg. Chem.*, 2008, **47**, 2243–2245.
- 10 F. Cisnetti, R. Guillot, M. Desmadril, G. Pelosi and C. Policar, *Dalton Trans.*, 2007, 1473–1476.
- 11 L. Garcia, S. Maisonneuve, J. Xie, R. Guillot, E. Rivière, M. Desmadril, F. Lambert and C. Policar, *Inorg. Chem.*, 2010, **49**, 7282–7288.
- 12 L. Garcia, S. Maisonneuve, J. O.-S. Marcu, R. Guillot, F. Lambert, J. Xie and C. Policar, *Inorg. Chem.*, 2011, **50**, 11353–11362.
- 13 F. Cisnetti, J.-D. Maréchal, M. Niaise, R. Guillot, M. Desmadril, F. Lambert and C. Policar, *Eur. J. Inorg. Chem.*, 2012, 3308–3319.
- 14 Z. Zhang, H. Harada, K. Tanabe, H. Hatta, M. Hiraoka and S. Nishimoto, *Peptides*, 2005, **26**, 2182–2187.
- 15 Y. Guminski, M. Grousseau, S. Cugnasse, V. Brel, J.-P. Annereau, S. Vispé, N. Guilbaud, J.-M. Barret, C. Bailly and T. Imbert, *Bioorg. Med. Chem. Lett.*, 2009, **19**, 2474–2477.
- 16 R. B. Katie, J. Blois, A. Smith, H. Yuan, F. Reynolds, R. Weissleder, L. C. Cantley and L. Josephson, *Bioconjugate Chem.*, 2008, **19**, 130–137.
- 17 U. Chatterjee, P. P. Bose, S. Dey, T. P. Singh and B. P. Chatterjee, *Glycoconjugate J.*, 2008, **25**, 741–752.
- 18 M. Zimmer, *Chem. Rev.*, 2002, **102**, 759–781.
- 19 A. R. Cowley, J. Davis, J. R. Dilworth, P. S. Donnelly, R. Dobson, A. Nightingale, J. M. Peach, B. Shore, D. Kerr and L. Seymour, *Chem. Commun.*, 2005, 845–847.
- 20 G. M. Chinigo, M. Paige, S. Grindrod, E. Hamel, S. Dakshanamurthy, M. Chruszcz, W. Minor and M. L. Brown, *J. Med. Chem.*, 2008, **51**, 4620–4631.
- 21 S. Maisonneuve, Q. Fang and J. Xie, *Tetrahedron*, 2008, **64**, 8716.
- 22 J.-M. Raimundo, P. Blanchard, H. Brisset, S. Akoudad and J. Roncali, *Chem. Commun.*, 2000, 939–940.
- 23 Y. Tian, W.-C. Wu, C.-Y. Chen, T. Strovas, Y. Li, Y. Jin, F. Su, D. R. Meldrum and A. K.-Y. Jen, *J. Mater. Chem.*, 2010, **20**, 1728–1736.
- 24 F. F. D. Oliveira, D. C. B. D. Santos, A. A. M. Lapis, J. R. Corrêa, A. F. Gomes, F. C. Gozzo, P. F. Moreira Jr, V. C. de Oliveira, F. H. Quina and B. A. D. Neto, *Bioorg. Med. Chem. Lett.*, 2010, **20**, 6001–6007.
- 25 B. A. D. Neto, P. H. P. R. Carvalho, D. C. B. D. Santos, C. C. Gatto, L. M. Ramos, N. M. de Vasconcelos, J. R. Corrêa, M. B. Costa, H. C. B. de Oliveira and R. G. Silva, *RSC Adv.*, 2012, **2**, 1524–1532.
- 26 T. Hamada and K. Yoshikawa, *Materials*, 2012, **5**, 2292–2305.
- 27 Y.-B. Ruan, Y. Yu, C. Li, N. Bogliotti, J. Tang and J. Xie, *Tetrahedron*, 2013, **69**, 4603–4608.
- 28 M. Martinez, L. Augsburg, T. Johnston and W. W. Jones, *Adv. Drug Delivery Rev.*, 2002, **54**, 805–824.
- 29 I. V. Tetko, V. Y. Tanchuk and A. E. P. Villa, *J. Chem. Inf. Comput. Sci.*, 2001, **41**, 1407–1421.
- 30 I. V. Tetko and V. Y. Tanchuk, *J. Chem. Inf. Comput. Sci.*, 2002, **42**, 1136–1145.
- 31 R. Dimova, S. Aranda, N. Bezlyepkina, V. Nikolov, K. A. Riske and R. Lipowsky, *J. Phys.: Condens. Matter*, 2006, **18**, S1151–S1176.
- 32 M. L. Berre, A. Yamada, L. Reck, Y. Chen and D. Baigl, *Langmuir*, 2008, **24**, 2643–2649.
- 33 M. I. Angelova and D. S. Dimitrov, *Faraday Discuss. Chem. Soc.*, 1986, **81**, 303–311.
- 34 A. Diguët, M. L. Berre, Y. Chen and D. Baigl, *Small*, 2009, **5**, 1661–1666.